

RESEARCH ARTICLE | AUGUST 08 2023

Temperature dependence of incommensurate modulation in $\text{Ca}_{0.28}\text{Ba}_{0.72}\text{Nb}_2\text{O}_6$

R. Beanland ; L. Harrison ; S. Khan ; T. Brown ; T. Roncal-Herrero ; H. Peirson ; A. P. Brown ; S. J. Milne 

 Check for updates

J. Appl. Phys. 134, 064101 (2023)

<https://doi.org/10.1063/5.0157636>


View
Online


Export
Citation

CrossMark

AIP Advances

Why Publish With Us?

 25 DAYS average time to 1st decision	 740+ DOWNLOADS average per article	 INCLUSIVE scope
---	--	---

[Learn More](#)

 AIP
Publishing

Temperature dependence of incommensurate modulation in $\text{Ca}_{0.28}\text{Ba}_{0.72}\text{Nb}_2\text{O}_6$

Cite as: J. Appl. Phys. 134, 064101 (2023); doi: 10.1063/5.0157636

Submitted: 15 May 2023 · Accepted: 17 July 2023 ·

Published Online: 8 August 2023



R. Beanland,^{1,a)} L. Harrison,¹ S. Khan,¹ T. Brown,² T. Roncal-Herrero,² H. Peirson,² A. P. Brown,² and S. J. Milne²

AFFILIATIONS

¹Department of Physics, University of Warwick, Coventry CV4 7AL, United Kingdom

²School of Chemical and Process Engineering, University of Leeds, Leeds LS2 9JT, United Kingdom

^{a)}Author to whom correspondence should be addressed: R.Beanland@warwick.ac.uk

ABSTRACT

We present an electron microscopy and diffraction study of a $\text{Ca}_x\text{Ba}_{1-x}\text{Nb}_2\text{O}_6$ ceramic with $x = 0.28$ (CBN28), a ferroelectric material with a partially filled tetragonal tungsten-bronze structure. The microstructure has strong similarities to that of $\text{Sr}_x\text{Ba}_{1-x}\text{Nb}_2\text{O}_6$, with an average orthorhombic symmetry and an intimate intermixture of merohedral twin variants at a length scale of tens of nanometers. Superstructure spots in diffraction patterns are displaced by a one-dimensional incommensurate modulation, characterized by a propagation vector $\delta\delta_0$. Heating experiments show that δ is strongly coupled to ferroelectric polarization, decreasing as 180° ferroelectric domains become more finely spaced and needle-like as the Curie temperature T_C is approached during heating and increasing once more above T_C . No change in symmetry is observed at T_C , consistent with a transition from ferroelectric to antiferroelectric (or ferrielectric) relaxor properties. The superstructure spots and incommensurate modulation disappear $\sim 250^\circ\text{C}$ above T_C , consistent with polar regions in the material becoming fully transient.

© 2023 Author(s). All article content, except where otherwise noted, is licensed under a Creative Commons Attribution (CC BY) license (<http://creativecommons.org/licenses/by/4.0/>). <https://doi.org/10.1063/5.0157636>

I. INTRODUCTION

$\text{Ca}_x\text{Ba}_{1-x}\text{Nb}_2\text{O}_6$ (CBN x), with a partially filled tetragonal tungsten-bronze (TTB) structure, is a uniaxial ferroic material of interest for dielectric,¹ non-linear optics,² and ferroelectric³ applications. Congruent melting occurs at $x = 0.28$, producing a thermally stable compound (CBN28) with a high Curie temperature T_C , typically reported to be between 250°C ³ and 275°C .⁴ Brillouin scattering and ultrasound observations indicate that it is a normal ferroelectric below T_C , transitioning to relaxor behavior above^{3,5} with polar nanoregions detectable up to $T^* \sim 530^\circ\text{C}$ and a Burns temperature $T_B \sim 800^\circ\text{C}$.⁶ Structurally, 180 DWs are found at room temperature, which become fine needles elongated along the polar axis as T_C is approached.⁷

Like other TTBs, CBN28 only adopts the prototype $P4/mbm$ (No.127) tetragonal structure ($a = b = 12.95 \text{ \AA}$, $c = 3.95 \text{ \AA}$) at high temperature. Below T_C , displacement of the Nb cation from the center of NbO_6 octahedra along the c -axis produces ferroelectricity, while coordinated distortions of the oxygen polyhedra reduce

symmetry still further.^{8–10} Furthermore, in CBN28,¹¹ like many other TTBs,¹² these distortions can couple to varying occupancies of the Ca and Ba sites with a period that is incommensurate with the crystal lattice. Initial studies of single crystal CBN^{4,11} denoted the average room temperature structure to be tetragonal with a doubled c -axis, with two incommensurate propagation vectors along $[110]$ and $[1\bar{1}0]$. However, several other TTBs have been found to be orthorhombic with unit cell $a_0 = 2\sqrt{2}a$, $b_0 = \sqrt{2}a$, $c_0 = 2c$ and only one incommensurate propagation vector.^{12,13} The almost perfect match $a_0 = 2b_0$ means that merohedral twins are common, leading to a pseudotetragonal cell found in macroscopic diffraction measurements. Here, using transmission electron microscopy (TEM) and electron diffraction, we show the same applies to CBN28.

The structural studies of Graetsch *et al.*⁴ found no change in symmetry at T_C for CBN28, proposing instead a transition from a polar ferroelectric state to an antiferroelectric, or almost non-polar ferrielectric, state. Polarizations of opposite sense are produced as one of the two sets of crystallographically distinct Nb cations move

28 November 2023 11:05:57

past the center of their NbO_6 octahedra, while the other set is unchanged and the incommensurate modulation remains. This is also consistent with the relaxor behavior above T_C with polar nano-regions that become gradually less stable with increasing temperature, becoming completely transient at a temperature T^* and non-existent above T_B . Here, using electron diffraction, we examine the incommensurate propagation vector as a function of temperature and find it reaches a minimum in reciprocal space at T_C , indicating a coupling between ferroelectricity and incommensurate modulation. The incommensurate modulation decreases above T_C and disappears at $\sim 200^\circ\text{C}$ above T_C , roughly consistent with other measurements of T^* in CBN28.^{5,6}

II. METHODS

CBN28 was produced by a conventional mixed oxide process similar to the undoped material in Peirson *et al.*¹ CaCO_3 (Alfa Aesar, 99.95%), BaCO_3 (Alfa Aesar, 99.95%), and Nb_2O_5 (Alfa Aesar, 99.9%) powders in appropriate quantities were dried at 200°C for >24 h and ball milled with yttria-stabilized zirconia milling media in isopropanol for 24 h. Dried, milled powders were calcined at 1200°C for 12 h in covered alumina crucibles. This extended calcination eliminated secondary phases, such as CaNb_2O_6 , seen in laboratory x-ray powder diffraction data from previous 4 h calcinations.¹

Specimens for TEM were prepared from the calcined powder, mixing a small amount with aluminum powder (particle size $<10\ \mu\text{m}$) in a ratio of $\sim 1:5$ in an aluminum foil wrap, which was then cold rolled to produce a solid Al sheet containing CBN28 particles. This sheet was then used as source material for conventional grinding, polishing, and Ar^+ ion milling to electron transparency. Specimens were examined in a JEOL 2100plus LaB_6 TEM operating at 200 kV. Heating experiments were performed with a Gatan 652 double tilt heating holder.

For clarity, all Miller indices are given in the reference frame of the prototype TTB structure.

III. RESULTS

We first demonstrate that merohedral twinning is present with incommensurate modulation in only one dimension. Selected area electron diffraction (SAED) patterns commonly show superstructure spots that are due to the cooperative rotations of the oxygen octahedral framework, as can be seen in the $[112]$ zone axis pattern of Fig. 1(b). In this pattern, the superstructure spots are close to $(2m+1)\frac{1}{2}1\bar{1}\bar{1} + \frac{n}{4}1\bar{1}0$, where m and n are integers, but are alternately displaced from those positions by $\pm\delta\delta_0$ to form pairs, such as that found in the circle of Fig. 1(b). This displacement is indicative of a structure with a period δ , incommensurate with the crystal lattice. In Fig. 1(b), $\delta = 0.054 \pm 0.002$, corresponding to a periodicity of 16.0 nm.

It is also possible to obtain SAED patterns from a single crystal with no (or extremely weak) superstructure reflections, as shown in Fig. 1(c). Using an objective aperture to form a dark field image using the superstructure spots shows the two regions quite clearly [Fig. 1(a)], with a dark region on the right of the image corresponding to an absence of superstructure spots. Interestingly, the bright region on the left shows a patchy contrast on a length scale of 10–50 nm. (Similar data obtained at the $[110]$ zone axis are shown in Fig. S11 of the supplementary material.) These observations are consistent with two orientational variants of an incommensurately modulated phase, with orthogonal components of a modulation vector along $[1\bar{1}0]$ or $[110]$, respectively.¹⁴ In such a case, the modulation vector of the second variant lies far from the Ewald sphere in Fig. 1(c), and only the first variant [Fig. 1(b)] can contribute to the dark field image, with the result that the second variant appears dark. The patchy contrast suggests that the two variants are intimately intermixed. These results are consistent with the SAED and high resolution TEM study of Lu *et al.*,¹⁵ who proposed an orthogonal cell for CBN28 with lattice parameters $a_O = 2\sqrt{2}a$, $b_O = \sqrt{2}a$, $c_O = 2c$. These data are also very similar to those presented by Krayzman¹³ in the TTB $\text{Sr}_{0.61}\text{Ba}_{0.39}\text{Nb}_2\text{O}_6$ (SBN61), suggesting a common structure and behavior. They

28 November 2023 11:05:57

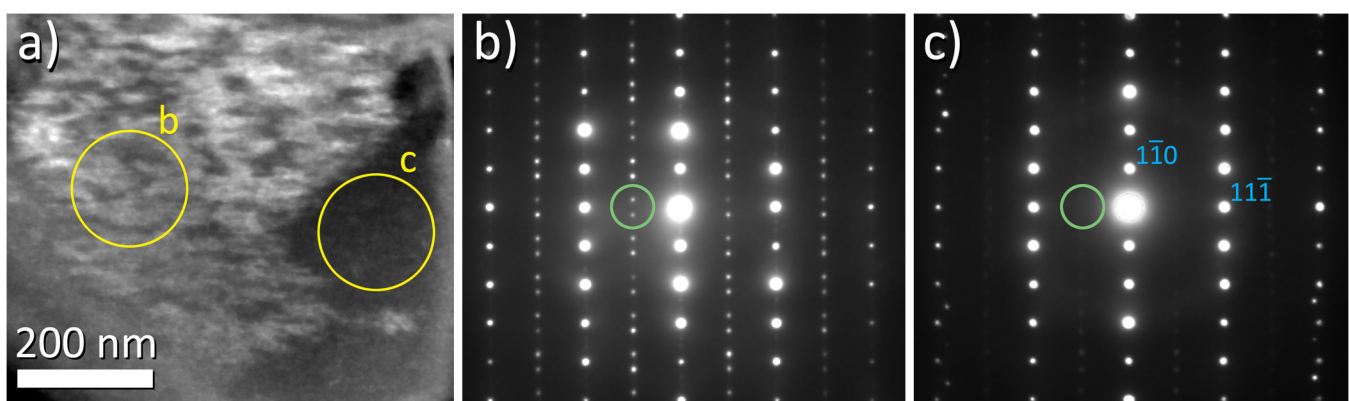


FIG. 1. (a) A dark field image of CBN28 obtained at the $[112]$ zone axis, using superstructure spots selected by an objective aperture placed at the position marked by the green circles in (b) and (c). Bright regions in (a) show areas of the material where superstructure spots are present, and dark regions show areas where they are absent. The SAED patterns in (b) and (c) were obtained using a selected area aperture located in the regions indicated by yellow circles in (a). Miller indices in (c) use the TTB prototype cell.

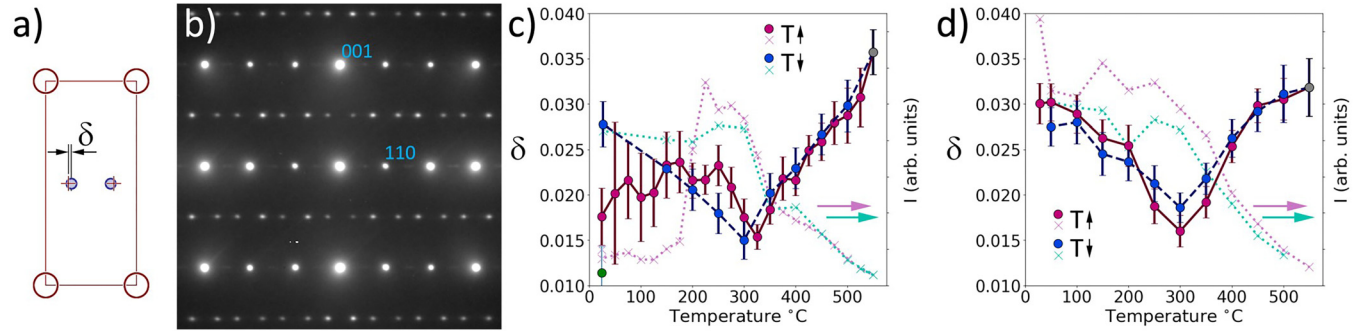


FIG. 2. (a) In a $[1\bar{1}0]$ SAED pattern from CBN28, superstructure spots are displaced from $h/4 k/4 (1 + 2l)/2$ positions by $\pm \delta\delta 0$ due to an incommensurate modulation. (b) A RT $[110]$ SAED pattern. Measured values of δ (left axis) and mean intensity of superstructure spots (right axis) are shown for (c) an initial and (d) a repeat heating cycle. Error bars are the standard deviation of 96 measurements of δ . The first measurement in (c) has two data points; the green point corresponds to a measurement made in the area denoted by the green circle in Fig. 3.

proposed that SBN61 consists of an intergrowth of two structures, one with unit cell $a' = 2\sqrt{2}a, b' = \sqrt{2}a, c' = 2c$ and a second with $a'' = 6\sqrt{2}a, b'' = \sqrt{2}a, c'' = 2c$. Together, these produce a phase mixture that results in an incommensurately modulated structure for each twin variant.

The behavior of the superstructure spots as a function of temperature in a $[1\bar{1}0]$ SAED pattern is shown in Fig. 2. In this pattern, superstructure spots are close to $h/4 k/4 (1 + 2l)/2$ (h, k, l integers) and are displaced by the same incommensurate propagation vector $\pm \delta\delta 0$ [Fig. 2(a)]. Two heating and cooling experiments

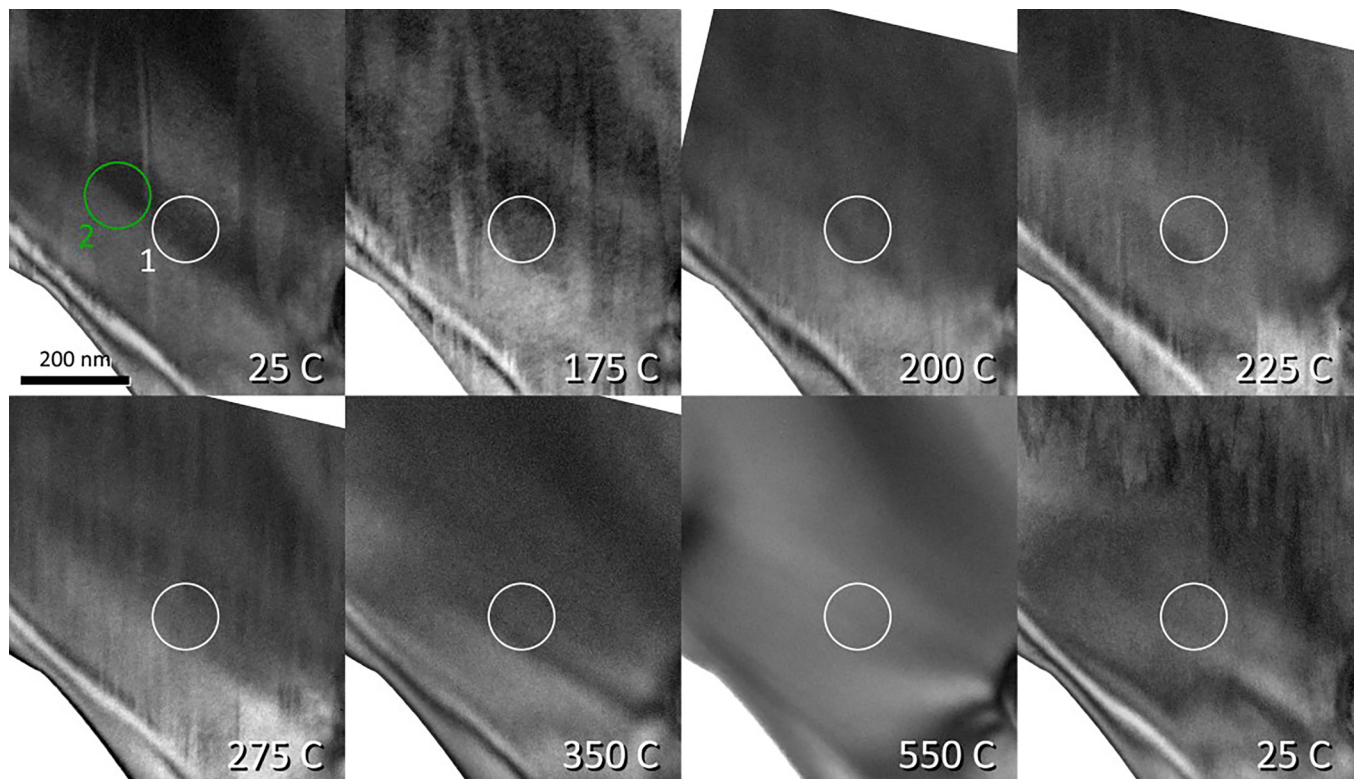


FIG. 3. Bright field $[1\bar{1}0]$ TEM images of the $[110]$ crystal used for the measurements in Fig. 2. The white circle shows the position of the selected area aperture. The green circle in the first image shows a second location, corresponding to the green data point in Fig. 2(c).

28 November 2023 11:05:57

were performed sequentially. Data analysis was performed using a Python script, measuring the position and intensity of 96 superstructure spots in each SAED pattern. Bright field TEM images, showing the position of the selected area aperture and the changing microstructure of the material during the first experiment, are shown in Fig. 3. At room temperature (25 °C), a domain structure is visible in the first image of Fig. 3. These are 180° ferroelectric domains.^{7,16} SAED patterns were taken from domains 1 and 2 in Fig. 3 and appeared essentially the same; however, more detailed analysis shows a significant difference in the value of δ , being $\delta_1 = 0.0175 \pm 0.0025$ and $\delta_2 = 0.0115 \pm 0.0025$. These values are rather less than the room temperature measurement of Lu¹⁵ of 0.0225 for single crystal material. During heating, the value of δ increased erratically up to a nominal temperature of ~250 °C, after which it dropped again. The intensity of the superstructure spots also behaved erratically, staying relatively low up to 200 °C where it increased dramatically. The images of Fig. 3 show the domain structure changes significantly during heating, with domain walls becoming denser and longer, aligned with the *c*-axis (vertical in these images) as observed previously in single crystal CBN28 by Lu *et al.*⁷ Evidence for decreasing domain size in CBN28 as T_C is approached, and a locally varying T_C that depends upon domain size has also been presented by Heine *et al.*¹⁷ using second harmonic generation.

The value of δ decreased until the domain structure vanished at ~300 °C. The absence of domains implies a loss of ferroelectricity, and we may, therefore, take this observation and the minimum value of δ to indicate at the Curie temperature T_C . Our bulk CBN28 ceramic has peak ϵ_r between ~240 and 268 °C,¹ in agreement with the documented values of T_C .^{4-6,18} Thus, the value of ~300 °C observed in Fig. 2 almost certainly results from the difference in the temperature measured at the thermocouple of the heating holder and the actual temperature of the crystallite at the edge of the thinned TEM specimen. The erratic rise observed in δ and its strong decrease as the domain size decreases suggests that the incommensurate modulation both interacts with the ferroelectric domains and varies in magnitude with the sign of polarization. Above T_C , δ increases linearly, while the intensity of the superstructure spots continues to decline. At 550 °C, $\delta = 0.035$, while the spots have almost vanished. On cooling, both δ and the superstructure spot intensities behave more regularly, with a sharp V in the value of δ and an increasing intensity as temperature drops. As can be seen in the final image of Fig. 3 at room temperature, while the domain structure has returned, the larger domains now do not extend to the thinnest part of the specimen where the diffraction pattern was taken. A very fine domain structure is still present, which is unresolved in this relatively low magnification image, but visible in higher magnification dark field images (supplementary Fig. SI2). The final value of δ at room temperature is 0.028.

This domain state was maintained for the second set of measurements, giving the repeatable data shown in Fig. 2(d). Above T_C , where the material is a relaxor,^{3,19} the intensity of the superstructure spots tends to zero at a nominal temperature of 600 °C. This corresponds well with ultrasound and Brillouin scattering measurements of the temperature T^* at which polar nanoregions become completely transient,^{3,5,6,19} taking into account the difference in the nominal temperature and the actual value at the position of

measurement. The well-behaved changes in intensity and δ in the second heating/cooling cycle are, therefore, probably a result of the fine domains in the material after the initial heating/cooling cycle. This subtle behavior is not readily apparent in macroscopic measurements since dielectric measurements of ceramics produced from the powder used in this TEM study showed no appreciable hysteresis or variations in behavior over successive heating cycles.

IV. DISCUSSION AND CONCLUSIONS

The ionic radius of Ca³⁺ with coordination number 12 is $r_{CN12} = 1.34 \text{ \AA}$, essentially the same as La³⁺.²⁰ Levin and co-workers²¹ showed that adding Nd to the filled mixed B-site TTB Nd_xLa_{1-x}Ba₂Ti₂Nb₃O₁₅ induced a change from incommensurate *Ama2* above T_C to a commensurate *Ima2* structure below, whereas the end-point compound LaBa₂Ti₂Nb₃O₁₅ (LBTN) showed no change, maintaining an incommensurate *Ama2* structure at all temperatures. The difference was ascribed to the smaller ionic radius of Nd³⁺ at $r_{CN12} = 1.27 \text{ \AA}$, an inference that was strengthened by subsequent work²² substituting other elements *M* to give MBa₂Ti₂Nb₃O₁₅, which gave a commensurate *Ima2* structure only for $r_{CN12} < 1.3 \text{ \AA}$. The lack of any phase change in CBN28, like LBTN, is, thus, in perfect agreement with these studies and the wider range of compounds surveyed by Zhu *et al.*¹²

In summary, these results are consistent with previous investigations of CBN28, with no change of symmetry observed at the Curie temperature T_C . The material has a microstructure closely related to that seen in SBN,¹³ with an average orthorhombic symmetry that presents as two intermixed (twin) variants at a scale of tens of nm. Each variant has a one-dimensional incommensurate modulation characterized by the propagation vector $\delta\delta 0$. The observation here that δ depends on the polarity of the material, couples to domain size below T_C , and the incommensurate modulation persists for ~250 °C above T_C indicates a strong coupling to polar modes in the material. While the presence of the incommensurate modulation in CBN28 above T_C has been noted,¹¹ its correlation with a domain structure has not been demonstrated until this work, and it would be interesting to investigate its behavior in related systems.

SUPPLEMENTARY MATERIAL

Additional data are given to support the images presented here. Figure SI1 reveals incommensurate spots and a dark field image of a [110] oriented crystal. Figure SI2 reveals dark field 002 images, showing 180° domains and their evolution during sample cooling.

ACKNOWLEDGMENTS

This work was funded by UKRI via the Engineering and Physical Sciences Research Council (EPSRC) at Warwick and Leeds (Award Nos. EP/V053701/1 and EP/S029036/1, respectively).

AUTHOR DECLARATIONS

Conflict of Interest

The authors have no conflicts to disclose.

Author Contributions

R. Beanland: Conceptualization (lead); Methodology (lead); Project administration (equal); Supervision (lead); Writing – original draft (lead). **L. Harrison:** Investigation (equal). **S. Khan:** Investigation (equal). **T. Roncal-Herrero:** Investigation (supporting). **H. Peirson:** Investigation (supporting). **S. J. Milne:** Funding acquisition (equal); Project administration (equal); Writing – review & editing (supporting).

DATA AVAILABILITY

The data that support the findings of this study are available within the article and its supplementary material.

REFERENCES

- ¹H. Peirson, J. Pan, Y. Li, D. A. Hall, A. P. Brown, R. M. Drummond-Brydson, and S. J. Milne, “Structure and dielectric properties of yttrium-doped $\text{Ca}_{0.28}\text{Ba}_{0.72}\text{Nb}_2\text{O}_6$ ceramics,” *J. Alloys Compd.* **950**, 169891 (2023).
- ²M. Eßer, M. Burianek, P. Held, J. Stade, S. Bulut, C. Wickleder, and M. Mühlberg, “Optical characterization and crystal structure of the novel bronze-type $\text{Ca}_x\text{Ba}_{1-x}\text{Nb}_2\text{O}_6$ ($x = 0.28$; CBN-28),” *Cryst. Res. Technol.* **38**, 457–464 (2003).
- ³S. Kojima, M. Aftabuzzaman, J. Dec, and W. Kleemann, “Brillouin scattering study of ferroelectric instability of calcium-strontium-barium niobate single crystals,” *Materials* **16**, 2502 (2023).
- ⁴H. Graetsch, J. Schreuer, M. Burianek, and M. Mühlberg, “Thermally induced structural changes in incommensurate calcium barium niobate $\text{Ca}_{0.28}\text{Ba}_{0.72}\text{Nb}_2\text{O}_6$ (CBN28),” *J. Solid State Chem.* **196**, 255–266 (2012).
- ⁵K. Suzuki, K. Matsumoto, J. Dec, T. Łukasiewicz, W. Kleemann, and S. Kojima, “Critical slowing down and elastic anomaly of uniaxial ferroelectric $\text{Ca}_{0.28}\text{Ba}_{0.72}\text{Nb}_2\text{O}_6$ crystals with tungsten bronze structure,” *Phys. Rev. B* **90**, 064110 (2014).
- ⁶C. S. Pandey, J. Schreuer, M. Burianek, and M. Mühlberg, “Anomalous elastic behavior of relaxor ferroelectric $\text{Ca}_{0.28}\text{Ba}_{0.72}\text{Nb}_2\text{O}_6$ single crystals,” *Phys. Rev. B* **84**, 174102 (2011).
- ⁷C. Lu, C. Nie, X. Duan, J. Li, H. Zhang, and J. Wang, “180 domain structure and its evolution in $\text{Ca}_{0.28}\text{Ba}_{0.72}\text{Nb}_2\text{O}_6$ ferroelectric single crystals of tungsten bronze structure,” *Appl. Phys. Lett.* **88**, 201906 (2006).
- ⁸M. Smirnov and P. Saint-Grégoire, “Unified approach for determining tetragonal tungsten bronze crystal structures,” *Acta Crystallogr. A* **70**, 283–290 (2014).
- ⁹T. A. Whittle, S. Schmid, and C. J. Howard, “Octahedral tilting in the tungsten bronzes,” *Acta Crystallogr. B* **71**, 342–348 (2015).
- ¹⁰B. Campbell, C. J. Howard, T. B. Averett, T. A. Whittle, S. Schmid, S. Machlus, C. Yost, and H. T. Stokes, “An algebraic approach to cooperative rotations in networks of interconnected rigid units,” *Acta Crystallogr. A* **74**, 408–424 (2018).
- ¹¹H. A. Graetsch, C. S. Pandey, J. Schreuer, M. Burianek, and M. Mühlberg, “Incommensurate modulation of calcium barium niobate (CBN28 and Ce: CBN28),” *Acta Crystallogr. B* **68**, 101–106 (2012).
- ¹²X. Zhu, M. Fu, M. Stennett, P. Vilarinho, I. Levin, C. Randall, J. Gardner, F. Morrison, and I. Reaney, “A crystal-chemical framework for relaxor vs normal ferroelectric behavior in tetragonal tungsten bronzes,” *Chem. Mater.* **27**, 3250–3261 (2015).
- ¹³V. Krayzman, A. Bosak, H. Y. Playford, B. Ravel, and I. Levin, “Incommensurate modulation and competing ferroelectric/antiferroelectric modes in tetragonal tungsten bronzes,” *Chem. Mater.* **34**, 9989–10002 (2022).
- ¹⁴L. Bursill and P. J. Lin, “Incommensurate superstructures and phase transition of strontium barium niobate,” *Acta Crystallogr. B* **43**, 49–56 (1987).
- ¹⁵C. J. Lu, Y. J. Qi, J. Q. Li, H. J. Zhang, and J. Y. Wang, “Incommensurate modulation structure in ferroelectric $\text{Ca}_{0.28}\text{Ba}_{0.72}\text{Nb}_2\text{O}_6$ single crystals of tungsten bronze structure,” *Appl. Phys. Lett.* **89**, 191901 (2006).
- ¹⁶X. He, L. Gu, and A. Rockett, “Scanning transmission electron microscopy imaging of 180° ferroelectric domains and application to $\text{Ca}_{0.28}\text{Ba}_{0.72}\text{Nb}_2\text{O}_6$ single crystals,” *Appl. Phys. Lett.* **109**, 262903 (2016).
- ¹⁷U. Heine, U. Voelker, K. Betzler, M. Burianek, and M. Muehlberg, “The ferroelectric phase transition of calcium barium niobate: Experimental evidence of Smolenskii’s model for diffuse phase transitions?,” *New J. Phys.* **11**, 083021 (2009).
- ¹⁸M. Eßer, M. Burianek, D. Klimm, and M. Mühlberg, “Single crystal growth of the tetragonal tungsten bronze $\text{Ca}_x\text{Ba}_{1-x}\text{Nb}_2\text{O}_6$ ($x = 0.28$; CBN-28),” *J. Cryst. Growth* **240**, 1–5 (2002).
- ¹⁹M. Aftabuzzaman, J. Dec, W. Kleemann, and S. Kojima, “Field dependent elastic anomaly in uniaxial tungsten bronze relaxors,” *Jpn. J. Appl. Phys.* **55**, 10TC01 (2016).
- ²⁰R. D. Shannon and C. T. Prewitt, “Effective ionic radii in oxides and fluorides,” *Acta Crystallogr. B* **25**, 925–946 (1969).
- ²¹I. Levin, M. C. Stennett, G. C. Miles, D. I. Woodward, A. R. West, and I. M. Reaney, “Coupling between octahedral tilting and ferroelectric order in tetragonal tungsten bronze-structured dielectrics,” *Appl. Phys. Lett.* **89**, 122908 (2006).
- ²²M. Stennett, I. Reaney, G. Miles, D. Woodward, A. West, C. Kirk, and I. Levin, “Dielectric and structural studies of $\text{Ba}_2\text{MTi}_2\text{Nb}_3\text{O}_{15}$ (BMTNO₁₅, M = Bi^{3+} , La^{3+} , Nd^{3+} , Sm^{3+} , Gd^{3+}) tetragonal tungsten bronze-structured ceramics,” *J. Appl. Phys.* **101**, 104114 (2007).